Collective firing patterns of neuronal networks with short-term synaptic plasticity

Chong-Yang Wang [1], Ji-Qiang Zhang [2,3], Zhi-Xi Wu,[1,*] and Jian-Yue Guan[1]

[1]*Lanzhou Center for Theoretical Physics and Key Laboratory of Theoretical Physics of Gansu Province, Lanzhou University, Lanzhou, Gansu 730000, China*

[2]*Beijing Advanced Innovation Center for Big Data and Brain Computing, Beihang University, Beijing 100191, China*

[3]*School of Physics and Electronic-Electrical Engineering, Ningxia University, Yinchuan 750021, China*

(Received 3 January 2020; revised 9 December 2020; accepted 28 January 2021; published 17 February 2021)

We investigate the occurrence of synchronous population activities in a neuronal network composed of both excitatory and inhibitory neurons and equipped with short-term synaptic plasticity. The collective firing patterns with different macroscopic properties emerge visually with the change of system parameters, and most long-time collective evolution also shows periodic-like characteristics. We systematically discuss the pattern-formation dynamics on a microscopic level and find a lot of hidden features of the population activities. The bursty phase with power-law distributed avalanches is observed in which the population activity can be either entire or local periodic-like. In the purely spike-to-spike synchronous regime, the periodic-like phase emerges from the synchronous chaos after the backward period-doubling transition. The local periodic-like population activity and the synchronous chaotic activity show substantial trial-to-trial variability, which is unfavorable for neural code, while they are contrary to the stable periodic-like phases. We also show that the inhibitory neurons can promote the generation of cluster firing behavior and strong bursty collective firing activity by depressing the activities of postsynaptic neurons partially or wholly.

DOI: 10.1103/PhysRevE.103.022312

I. INTRODUCTION

A vast variety of cortical activities with remarkable features are ubiquitously observed *in vitro* and *in vivo*, such as irregular activity [1,2], neuronal avalanches [3–5], and synchronous oscillations [6–8]. Irregular spiking patterns are found to be related to an approximate balance between excitatory and inhibitory inputs, and it is an emergent network property that does not necessarily depend on intricate cellular mechanisms [9,10]. Neuronal avalanches are shown by the power-law forms with exponents $-3/2$ and -2 of the avalanche size and duration distributions by measuring the spontaneous activity on slices of neuronal cultures [3,11]. Such scale-invariant neuronal dynamics can be reached by neuronal activities closely near a critical point (which is related to self-organized criticality) [12–14], or in an extended critical-like region (the Griffiths phase) [15]. Moreover, the power-law neuronal avalanches have been demonstrated to optimize the computational capabilities [16], the transmission and storage of information [17,18], the dynamical response range, and the sensitivity to sensory stimuli [19–21]. The criticality of cortical networks is still a conundrum and has attracted a lot of attention [22–24].

Studies of synchronous oscillation have been an active area in a lot of research domains, including physics, mathematics, biology, ecology, etc. [25,26]. The occurrence of synchronous oscillations emerges from various mechanisms, which have received a great deal of attention in diverse subjects. In the field of neuroscience, synchronous oscillations reveal the essential mechanism of the temporal coordination of neuronal activities, which have been considered to be crucial for several cognitive capacities [27]. For example, the theta oscillations (4–8 Hz) play a role in the formation and retrieval of episodic memory [28], the beta oscillations (15–30 Hz) are associated with behavioral stopping in the motor system [29], and the gamma oscillations (30–80 Hz) subserve a fundamental process in cortical computation [30]. What is more, synchronous oscillations are also integrated with pathophysiology, where abnormal strong or weak synchronous oscillatory activities of neurons may indicate some diseases, such as epileptic seizures, schizophrenia, and Alzheimer's disease [31–33]. It is now broadly accepted that some of the disease-related alterations of neurotransmitter systems interfere directly with the mechanisms that support different degrees of synchronous oscillations [33]. Consequently, the in-depth study of neuronal synchronization of the joint activity of multiple neurons plays a significant role in the understanding of neural information processing and the effective diagnosis and therapy of brain diseases.

Nowadays, neuroscientists have identified that a chemical synapse is crucial in signal transmission for most neurons. It acts through the diffusion of a neurotransmitter as soon as an action potential (or spike) from a presynaptic neuron arrives at it. Briefly, chemical synaptic transmission occurs by translating the action potential from presynaptic neurons into the chemical signal at the synapses, and further into an electrical response at the postsynaptic side [34,35]. Such activity-dependent synaptic transmission is successfully mimicked by the Tsodyks-Uziel-Markram (TUM) model [36–38],

*wuzhx@lzu.edu.cn

and it has been invoked to explain a large number of synchronous oscillations in cortical networks [39–43]. Most of the previous research provides an effective analysis method to reproduce synchronous patterns in experiments [36,44]. However, the complicated interaction between excitatory and inhibitory neurons underlying synchronous neuronal activities is always an immensely complex task, and there are still several problems that need to be fully explored. In this paper, we focus on the neuronal networks composed of adaptive exponential integrate-and-fire excitatory neurons and standard leaky integrate-and-fire inhibitory neurons, interacting via synaptic currents regulated by the short-term synaptic plasticity. We try to give a comprehensive perspective of the collective firing population activities with diverse macroscopic or microscopic properties, and we provide a clear explanation of the pattern-formation dynamics, including how the short-term synaptic plasticity promotes the occurrence of synchronous oscillations and how synaptic inhibition from inhibitory neurons influences the population activity of a large population of neurons.

The paper is organized as follows. In Sec. II, we describe the neuronal models of both excitatory and inhibitory neurons, the synaptic currents with short-term depression, and facilitation of synaptic transmission. We also present the details of the simulations and the statistical indicators used in our paper. In Sec. III, we show the collective firing patterns with different macroscopic properties, and we systematically explore the pattern-formation dynamics with the change of the system parameters on a microscopic level. Finally, we give a brief summary and discussion of our main results in Sec. IV.

II. MODEL AND METHOD

We consider a neuronal network composed of $N_E = 8000$ excitatory neurons and $N_I = 2000$ inhibitory neurons so that the fraction of inhibitory neurons is equal to 0.2 in accordance with the experimental observation [46,47]. The presynaptic neurons of a postsynaptic neuron are $k_E = 400$ excitatory neurons and $k_I = 100$ inhibitory neurons randomly selected from excitatory and inhibitory neurons, respectively. Thus each neuron has $k = k_E + k_I = 500$ presynaptic neurons, as sketched in Fig. 1(a). The dynamics of the membrane potentials of excitatory and inhibitory neurons and the synaptic currents from presynaptic neurons to postsynaptic neurons are expatiated below.

A. Membrane potential dynamics

The membrane potentials of excitatory neurons are modeled by the adaptive exponential integrate-and-fire model extracted from experimental data, which are described by the following differential equation [48–50]:

$$\frac{dV_i^E(t)}{dt} = -\frac{1}{\tau_m}\left[V_i^E(t) - V_{\rm rest}^E\right] + \frac{I_i^{E,\rm ext}}{C} + \frac{I_i^{\rm syn}}{C} + \frac{\Delta_T}{\tau_m}\exp\left(\frac{V_i^E(t) - V_{T,i}^E(t)}{\Delta_T}\right) - \frac{w_i(t)}{C}, \quad (1)$$

where τ_m is the membrane time constant, $V_{\rm rest}^E$ is the resting potential of the excitatory neuron, C is the membrane capacitance, $I_i^{E,\rm ext}$ is an external input current to the excitatory neuron i, $I_i^{\rm syn}$ is the total synaptic current received by neuron i, Δ_T is the spike slope factor, and the neuronal threshold $V_{T,i}^E(t)$ evolves according to

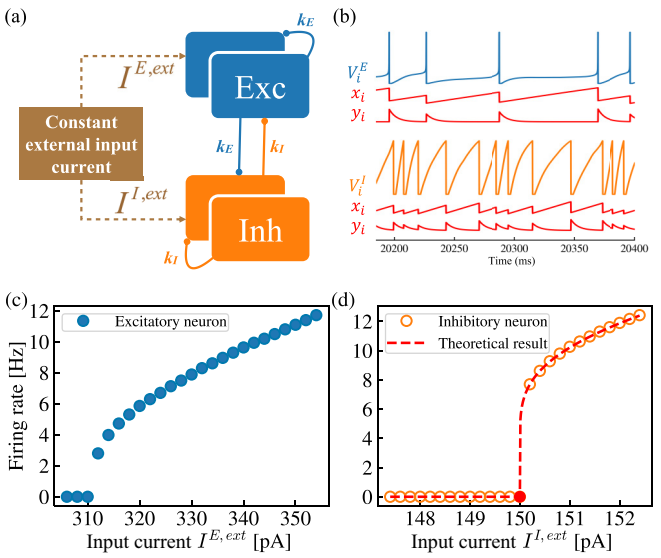

FIG. 1. (a) Schematic representation of a neuronal network consisting of both excitatory (Exc) and inhibitory (Inh) neurons. The neurons are coupled by excitatory [blue (dark gray) lines] and inhibitory [orange (gray) lines] synaptic connections. The solid points at the ends of the lines indicate the synapses. The brown dashed lines with arrows represent the external drives. (b) Time series of membrane potentials V_i^α, available neurotransmitters x_i, and active neurotransmitters y_i of a randomly selected excitatory neuron (top, $\alpha = E$) and an inhibitory neuron (bottom, $\alpha = I$). The membrane potentials have been cut off at the firing threshold in each spike. (c), (d) Gain functions of (c) a free-running excitatory neuron and (d) a free-running inhibitory neuron. The red dashed line in (d) is the theoretical result given by Eq. (S7) in the Supplemental Material [45]. The red point is the critical point $I^{I,\rm ext} = 150$ pA, which separates the resting states and the active states.

$$\frac{dV_{T,i}^E(t)}{dt} = \frac{1}{\tau_T}\left[V_{\rm th} - V_{T,i}^E(t)\right], \quad (2)$$

where τ_T is the adaptive threshold timescale, and $V_{\rm th}$ is the threshold potential. Whenever neuron i fires, its neuronal threshold $V_{T,i}^E(t)$ is set to $V_{\rm th} + A_T$. The spike-triggered adaptation current $w_i(t)$ is given by

$$\frac{dw_i(t)}{dt} = \frac{1}{\tau_w}\left\{a_w\left[V_i^E(t) - V_{\rm rest}^E\right] - w_i(t)\right\} + b_w\mathscr{S}_i(t), \quad (3)$$

where τ_w is a time constant, a_w is the level of subthreshold adaptation, $\mathscr{S}_i(t) = \sum_f \delta(t - t_i^f)$ is the spike train of neuron i, t_i^f is the firing time of neuron i, and f is the label of the spike. When a neuron fires, its adaptation current is increased by an amount b_w.

Here, we model the inhibitory neurons as the standard leaky integrate-and-fire neurons, whose dynamics of the membrane potentials are given by [50,51]

$$\frac{dV_i^I(t)}{dt} = -\frac{1}{\tau_m}\left[V_i^I(t) - V_{\rm rest}^I\right] + \frac{I_i^{I,\rm ext}}{C} + \frac{I_i^{\rm syn}}{C}, \quad (4)$$

where V_{rest}^{I} is the resting potential of the inhibitory neuron, and $I_i^{I,\text{ext}}$ an external input current to the inhibitory neuron i.

Each postsynaptic excitatory (inhibitory) neuron integrates the synaptic currents from all its presynaptic neurons and the external input current $I_i^{E,\text{ext}}$ ($I_i^{I,\text{ext}}$). The external input current represents the background response in the brain, inputs from other brain regions, the external stimuli, etc. For the sake of convenience, the external input current is regarded as constant in our work, $I_i^{\alpha,\text{ext}} = I^{\alpha,\text{ext}}$, as illustrated in Fig. 1(a). When the membrane potential of an excitatory (inhibitory) neuron reaches the firing threshold θ^E (θ^I), the neuron emits a spike and its potential is reset to the reset potential V_{r} and remains unchanged until passing through an absolute refractory period τ_{ref}. Notice that the membrane potential of each excitatory neuron has a rapid upswing to infinity in an incredibly short time, but that of the inhibitory neuron shows slow growth. Thus the response of an excitatory neuron is more immediate than an inhibitory one when they are near the firing threshold [see Fig. 1(b)].

B. Synaptic current

Following the TUM model [36–38], the effective synaptic strength from presynaptic neuron to postsynaptic neuron is determined by the faction of active synaptic resources on each synapse. In our paper, we consider a simplified version in which the neurotransmitter resources in each neuron are equally shared by all the postsynaptic neurons [39,52]. In detail, the neurotransmitter resources of neuron i are divided into three states: available with fraction $x_i(t)$, active with fraction $y_i(t)$, and inactive with fraction $z_i(t)$, $x_i(t) + y_i(t) + z_i(t) = 1$. The dynamics of these neurotransmitters are described as follows:

$$\frac{dx_i(t)}{dt} = \frac{z_i(t)}{\tau_r} - u_i(t)x_i(t)\mathscr{S}_i(t), \tag{5a}$$

$$\frac{dy_i(t)}{dt} = -\frac{y_i(t)}{\tau_{in}} + u_i(t)x_i(t)\mathscr{S}_i(t), \tag{5b}$$

$$\frac{dz_i(t)}{dt} = \frac{y_i(t)}{\tau_{in}} - \frac{z_i(t)}{\tau_r}, \tag{5c}$$

where τ_{in} is the characteristic decay time of the active neurotransmitter, and τ_r is the recovery time of the available neurotransmitter from the inactive neurotransmitter. These equations describe the short-term depression of the synaptic plasticity. When neuron i fires, its active neurotransmitter $y_i(t)$ increases to a large value abruptly, and concurrently it delivers synaptic currents to its postsynaptic neurons [see Fig. 1(b)].

The short-term facilitation of both excitatory and inhibitory neurons is also introduced by the changeable release fraction $u_i(t)$ of available neurotransmitter resources, which depends on the intracellular calcium concentration in physiology [53,54],

$$\frac{du_i(t)}{dt} = \frac{U - u_i(t)}{\tau_{\text{fac}}} + U[1 - u_i(t)]\mathscr{S}_i(t), \tag{6}$$

where U is the release fraction at rest, and τ_{fac} is the characteristic time.

The total synaptic current received by the neuron i in Eqs. (1) and (4) is the summation of the currents from both excitatory and inhibitory presynaptic neurons,

$$I_i^{\text{syn}} = \sum_{p=1}^{N_E} A\epsilon_{ip}y_p(t) - g\sum_{q=1}^{N_I} A\epsilon_{iq}y_q(t), \tag{7}$$

where A is the strength of synaptic efficacy, modeled as the maximum postsynaptic current which can be generated by activating all neurotransmitter resources, and g is the relative inhibitory efficacy. ϵ_{ij} is the connectivity matrix, whose entry is equal to 1 if there is a connection from the presynaptic neuron j to the postsynaptic neuron i, and 0 otherwise.

C. Details of the simulations and the statistical indicators

The gain functions of single excitatory and inhibitory neuron in Figs. 1(c) and 1(d) show the firing rate of a free-running neuron versus the constant external input current in the absence of synaptic current. Clearly, a neuron never becomes active with low external input current until passing through a critical point, and then it fires periodically with a fixed firing rate due to the summation process of the external input current and the reset process of the membrane potential. In this paper, we will study a neuronal network where the excitatory neurons are suprathreshold (with external drive greater than the critical point), while the inhibitory ones are exactly at the critical point [see Fig. 1(d)]. The system thereby can be considered as a master-slave system. The excitatory neurons fire spontaneously and drive the evolution of the whole system. Meanwhile, the activities of inhibitory neurons will depress the postsynaptic neurons.

The parameters for neuronal membrane dynamics and synaptic current used in our simulations can be found in Appendix A (Tables I and II). The dynamics of the neurons are integrated numerically by using the Euler method with a fixed time step of $\Delta t = 0.1$ ms. In our simulations, we let the system evolve for 40 s and then measure the quantities in the next 60 s.

To characterize the population activity of the neurons, we measure the average membrane potential at time t,

$$\bar{V}_\alpha(t) = \frac{1}{N_\alpha}\sum_{i=1}^{N_\alpha} V_i^\alpha(t), \tag{8}$$

the average synaptic fields [39]

$$Y_\alpha(t) = \frac{1}{N_\alpha}\sum_{i}^{N_\alpha} y_i(t), \quad Z_\alpha(t) = \frac{1}{N_\alpha}\sum_{i}^{N_\alpha} z_i(t), \tag{9}$$

the average firing rate r_α, and the instantaneous population spike rate (IPSR) $R_\alpha(t)$ of both excitatory ($\alpha = E$) and inhibitory ($\alpha = I$) neurons. The IPSR $R_\alpha(t)$ is conventionally used to visualize the synchronous oscillations, which are estimated by convoluting the spike train $\mathscr{S}_i(t)$ with a kernel $\psi_h(s)$ [55–57],

$$R_\alpha(t) = \frac{1}{N_\alpha}\sum_{i}^{N_\alpha}\int \mathscr{S}_i(t-s)\psi_h(s)ds, \tag{10}$$

and the kernel used here is the Gaussian density function with bandwidth h,

$$\psi_h(s) = \frac{1}{\sqrt{2\pi}h}\exp\left(-\frac{s^2}{2h^2}\right), \quad -\infty < s < \infty. \tag{11}$$

It is worth pointing out that an oscillating curve of the IPSR can be obtained in the synchronous case with collective firing activity, whose temporal patterns display stripe property [57].

The regularity of individual spikes can be characterized by the coefficients of variation (CV) of the interspike interval (ISI) distribution,

$$\mathrm{CV}_i = \sigma^i_{\mathrm{ISI}} \big/ \langle \mathrm{ISI}^f_i \rangle^i_f, \tag{12}$$

where $\langle \mathrm{ISI}^f_i \rangle^i_f$ and σ^i_{ISI} are the mean and the standard deviation of ISIs of neuron i. For the total neuronal network, we use the average CV to measure the regularity of individual activities throughout the population in each group, $\mathrm{CV}_\alpha = \langle \mathrm{CV}_i \rangle_\alpha$ [8]. The individual activities are regular with CV_α close to 0, irregular with CV_α near 1, and bursting with CV_α much larger than 1.

In addition, we use the synchronization index S_α to quantify the synchronization of the population activity [58]

$$S_\alpha = \frac{\langle \bar{V}_\alpha(t)^2 \rangle_t - \langle \bar{V}_\alpha(t) \rangle_t^2}{\sum_{i=1}^{N_\alpha} \left[\langle V_i(t)^2 \rangle_t - \langle V_i(t) \rangle_t^2 \right] / N_\alpha}, \tag{13}$$

where $\langle \cdot \rangle_t$ denotes the time average. The synchronous population activity is related to a finite value of S_α, and the larger the value of S_α is, the more synchronous are the neurons.

Since information is encoded in the spike train rather than in the form of an action potential, we also use the Kuramoto parameter to characterize the spike-to-spike synchronization, which just concerns the uniformity of the phase of spikes [39,59],

$$K_\alpha = \left\langle \left| \frac{1}{N_\alpha} \sum_i^{N_\alpha} e^{j\eta_i^f} \right| \right\rangle_t, \quad \eta_i^f(t) = 2\pi \frac{t - t_i^f}{t_i^{f+1} - t_i^f}, \tag{14}$$

where j is the imaginary unit and $\eta_i^f(t)$ is the phase of neuron i at time $t \in [t_i^f, t_i^{f+1}]$. $K_\alpha = 1$ indicates that the firing events are perfectly synchronous, and the synchronization is progressively lost with the decrease of K_α.

III. RESULTS

The population activities are characterized by the statistical indicators in the parameter space of synaptic efficacy A and relative inhibitory efficacy g [see Appendix B (Fig. 9)]. The neurons fire intensively in the regions with either small g or small A, and they are suppressed in the region with large g and large A. The statistical indicators oscillate with the change of the parameters, which indicates the switch process of various population activities. To investigate the temporal behavior of population activities systematically, we fix the relative inhibitory efficacy $g = 0.5$, and we study the *firing patterns* by tuning the synaptic efficacy A (see Fig. S2 in the Supplemental Material [45]) [60]. Figures 2(a)–2(c) show that the average firing rates r_α, the synchronization indexes S_α, and

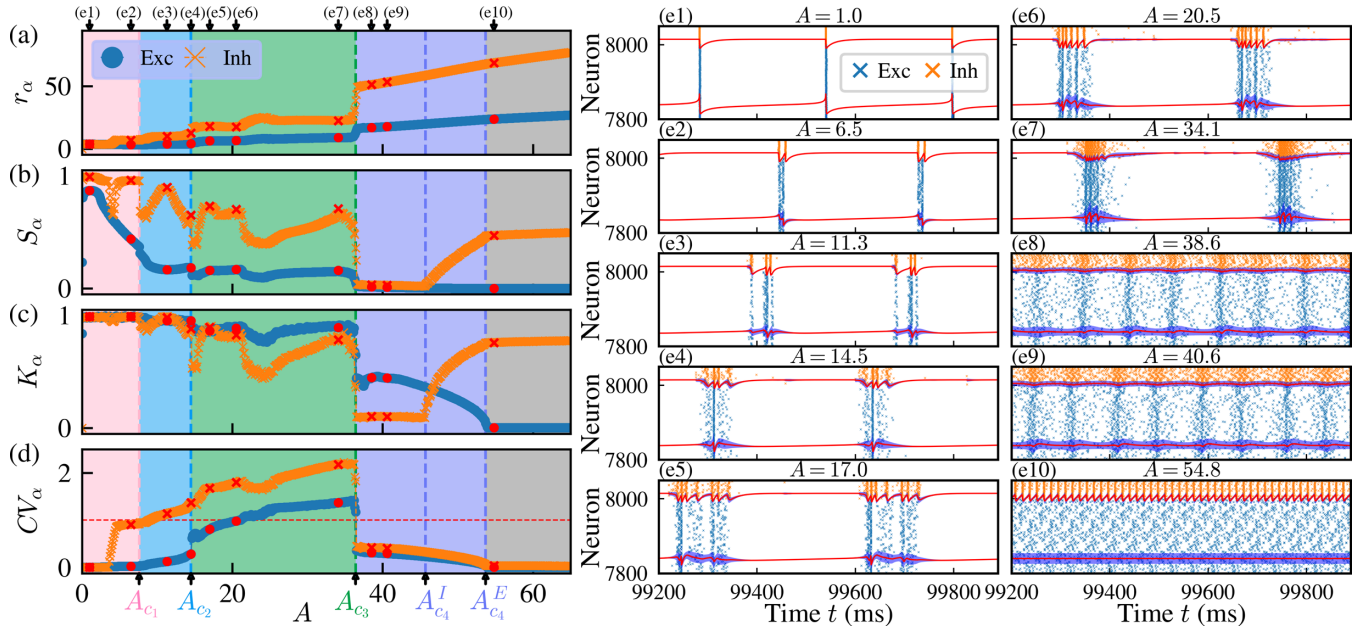

FIG. 2. (a) Average firing rates r_α, (b) synchronization indexes S_α, (c) Kuramoto parameters K_α, and (d) average coefficients of variation CV_α of the interspike interval (ISI) distribution of excitatory (Exc, $\alpha = E$) and inhibitory (Inh, $\alpha = I$) neurons with relative inhibitory efficacy $g = 0.5$. A_{c_1}, A_{c_2}, A_{c_3}, and $A^\alpha_{c_4}$ are the transition points which separate the parametric regions with similar pattern-formation dynamics. (e1)–(e10) Raster plots for different synaptic efficacy A [the red points in (a)–(d) and the parameters A in (e1)–(e7) correspond to the maxima of the curve S_I] with fixed $g = 0.5$. Neurons 7800–8000 are excitatory and neurons 8001–8050 are inhibitory. The red lines denote the average membrane potential $\bar{V}_\alpha(t)$. The blue shaded regions around the average membrane potential are the standard deviations. The constant external input currents of excitatory and inhibitory neurons are $I^{E,\mathrm{ext}} = 314$ pA and $I^{I,\mathrm{ext}} = 150$ pA, respectively.

the Kuramoto parameters K_α do not change monotonically with A. The oscillation shows lots of sharp jumps (indicated by the positions of A_{c_1}, A_{c_2}, A_{c_3}, and $A^{\alpha}_{c_4}$) with the increase of A for excitatory and inhibitory neurons, either separately or jointly, and they separate the regions with similar pattern-formation dynamics [see Figs. 2(a)–2(d) and the analysis in Appendix C (Fig. 10)]. Specifically, the curves of S_α and K_α show that the population activities are synchronous with both membrane potentials and spikes in the region $A \leqslant A_{c_3}$. The following results in Sec. III B shown below indicate that the avalanche distributions of the cascading activities between the collective firing activities in the bursty regime are power-law with an exponential cutoff when $A_{c_1} < A \leqslant A_{c_2}$ and are of perfect power-law form when $A_{c_2} < A \leqslant A_{c_3}$. Moreover, in the region $A_{c_3} < A \leqslant A^{\alpha}_{c_4}$, where S_α tends to zero while K_α has a finite value, the neurons only synchronize with spikes, and such a phenomenon is termed *pure spike-to-spike synchronization* in this paper.

The time series of spikes in Figs. 2(e1)–2(e10) indicate that various oscillatory firing patterns can be realized with different synaptic efficacy A. The collective firing activity displays an obvious stripe. Every maximum of S_α or K_α corresponds to a relatively clear synchronous pattern with a different number of stripes, and the number of stripes in a firing pattern increases with the enhancement of neuronal activity. The patterns between them display relatively weak synchronization with sparse and smeared stripes. Moreover, those patterns with multiple stripes imply the emergence of (regular or irregular) synchronous oscillations that are mixed with both low and high firing frequencies.

In most population activities, the long-term series of spikes show that the population activities are periodic-like. According to previous studies [39], the periodic characteristic of collective motion can be confirmed by the perfect closed trajectories of average synaptic fields [$Y_\alpha(t)$ versus $Z_\alpha(t)$, termed *global attractors* of the population activities]. In our work, the temporal fluctuation of the cascading activities in the region $A > A_{c_1}$ leads to a finite fluctuation around the lines of the global attractors (see Fig. S3 in the Supplemental Material [45]). This phenomenon demonstrates that microscopic chaos exists in the population activity, which successfully depicts the variability of neuronal activity in experiments [2,61]. The macroscopic population activity still has a periodic-like characteristic under the small fluctuation in most situations.

In the following, we probe the pattern-formation dynamics and the switch processes of the different firing patterns with the increase of A on a microscopic level. Interestingly, several microscopic features of the population activities can be observed, including two different types of cluster firing behaviors; the bursty population activity featuring power-law-distributed neuronal avalanches of the cascading activity; the pure spike-to-spike synchronous population activities, which are synchronous chaotic or periodic-like with period 4, 2, 1; etc.

A. Periodic collective firing activity and cluster firing behavior under the weak-coupling condition

Under the weak-coupling condition ($A \leqslant A_{c_1}$), the synaptic interactions among neurons are not too strong to significantly influence the neuronal activities of postsynaptic neurons. The perfectly periodic collective firing activities arise due to the slow adaption process of the input currents and the reset processes of the membrane potentials, which effectively reduces the phase difference between postsynaptic neurons. As A increases, the population activities switch from the firing patterns with only one stripe to those with two stripes [see Figs. 2(e1)–2(e2) and the illustrations in Fig. 3(b)]. In these population activities, there is always a long inactive period between two continuous collective firing stripes. The active neurotransmitters decay to the lowest levels gradually in these periods. Then some excitatory neurons will fire ahead due to the external drive. After that, the inhibitory neurons will fire collectively in a rapid manner, since they are subthreshold with the intrinsic dynamical property and are sensitive to synaptic excitation. Thus the collective firing activity of inhibitory neurons is slightly ahead of the activity of excitatory ones, which is indicated by the delay time Δ_τ between the collective firing stripe of inhibitory neurons and that of excitatory neurons [calculated by the interval between the maxima of IPSRs $R_I(t)$ and $R_E(t)$; see Figs. 3(a) and 3(b)]. Moreover, the delay time Δ_τ shortens with the enhancement of the synchronization of either excitatory or inhibitory neurons.

With the further increase of A, excitatory neurons that are far away from the firing threshold will be depressed by the synaptic inhibition and fire collectively themselves in a separate stripe. Then in the next firing pattern these neurons fire early and form the first stripe, because they do not respond to

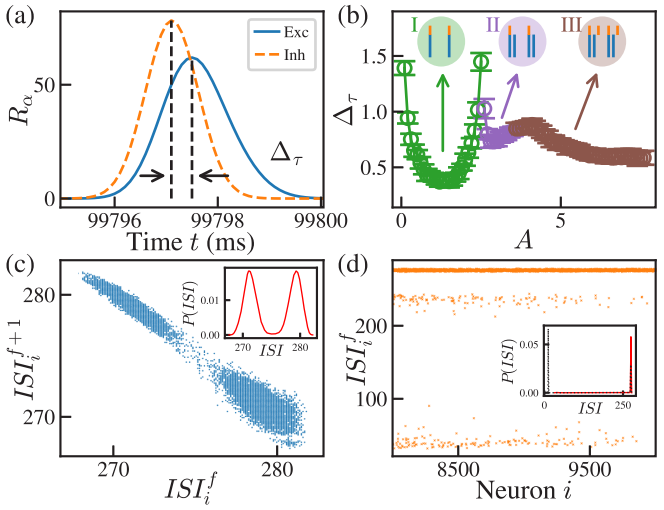

FIG. 3. (a) Illustration for the calculation of the delay time Δ_τ between the collective firing stripes of inhibitory and excitatory neurons at the beginning of each firing pattern by the maximum of the IPSR $R_\alpha(t)$ with $A = 1.0$. (b) Delay time Δ_τ vs synaptic efficacy A with three different cases: (I) the firing patterns of both excitatory and inhibitory neurons have only one stripe; (II) the firing patterns of excitatory neurons have two stripes, while those of inhibitory neurons have only one stripe; (III) the firing patterns of both excitatory and inhibitory neurons have two stripes. (c) Interspike-interval (ISI) return map of excitatory neurons, and (d) the ISIs of inhibitory neurons with $A = 3.6$. Inset: ISI distributions with $A = 3.6$ [solid lines in (c) and (d)] and $A = 7.6$ [dotted line in (d)]. ISI_i^f is the ISI between the fth and $(f+1)$th spikes of neuron i.

the inhibitory currents when they are in the absolute refractory periods. Thus the excitatory neurons fire with a long ISI and a short ISI alternately, and they are divided into clusters [see the ISI return map in Fig. 3(c)]. Their population activity displays the feature of *cluster firing* (two-cluster states), which shows that the neurons split into groups, and in each group they fire collectively, whereas a nonzero phase shift exists between different groups [62]. Briefly, such a switch process from the firing pattern with one stripe to that with two stripes of excitatory neurons is caused by the synaptic inhibition from presynaptic inhibitory neurons. Noticeably, the switch process of inhibitory neurons shows different behavior. After the collective firing of all excitatory neurons, synaptic excitation increases to a large value quickly. When A is large enough, some inhibitory neurons will fire again in a short time due to the slow decay of active neurotransmitter and the persistent external drive. And such a small group of inhibitory neurons is not fixed but can be any inhibitory neuron [see Fig. 3(d)], which is caused by the temporal fluctuations of membrane potentials and synaptic currents. With the increase of A, the small group of inhibitory neurons grows until all inhibitory neurons fire again [see the ISI distribution $P(\mathrm{ISI})$ of the inhibitory neurons with two maxima in the inset of Fig. 3(d)] and the population activity reaches a strong synchronous state.

B. Bursty population activity with power-law distributed neuronal avalanches

In the region $A_{c_1} < A \leqslant A_{c_2}$, the number of firing excitatory neurons (which fire ahead in the inactive periods to drive the neuronal cascades; these neurons will be called *pioneers* hereafter as in the work by Touboul [63]) increases and the inhibitory neurons will fire more intensively. The rest of the excitatory neurons are depressed by the synaptic inhibition within a long time interval, and then they fire in a cascading way as a result of the temporal fluctuations of membrane potentials and synaptic inputs [see Fig. 2(e3)]. The excitatory neurons in these population activities can be divided into two categories: one is the small group of pioneers, and the other is the remaining neurons depressed by the synaptic inhibition (which can be classified by the ISIs). This population activity also shows the feature of cluster firing, but the microscopic properties are different from those in the case of the weak-coupling condition [64]. Moreover, the population spikes over time are divided into groups that are separated by inactive periods [these groups are defined as *spike avalanches*; see Figs. 2(e3) and 2(e4)]. It is noticeable that the events with large avalanche sizes and long avalanche durations happen with large probabilities, which correspond to the collective firing activities. By removing these avalanche events, the avalanche size distributions $P(L_\alpha)$ and the avalanche duration distributions $P(D_\alpha)$ can be approximated by the following expressions:

$$P(L_\alpha) \sim L_\alpha^{-\gamma_{L_\alpha}} e^{-\lambda_{L_\alpha} L_\alpha}, \tag{15}$$

$$P(D_\alpha) \sim D_\alpha^{-\gamma_{D_\alpha}} e^{-\lambda_{D_\alpha} D_\alpha}, \tag{16}$$

which are the power-law distributions with an exponential cutoff [12]. As shown in Fig. 4, the fitting results obtained by the least-squares-fitting method agree well with the simulation results. The results in the Supplemental Material also show that the exponents λ_L, λ_D decrease with the increase of A, which implies that the distributions will get close to the power-law forms gradually (see Fig. S5 and Table SI in the Supplemental Material [45]).

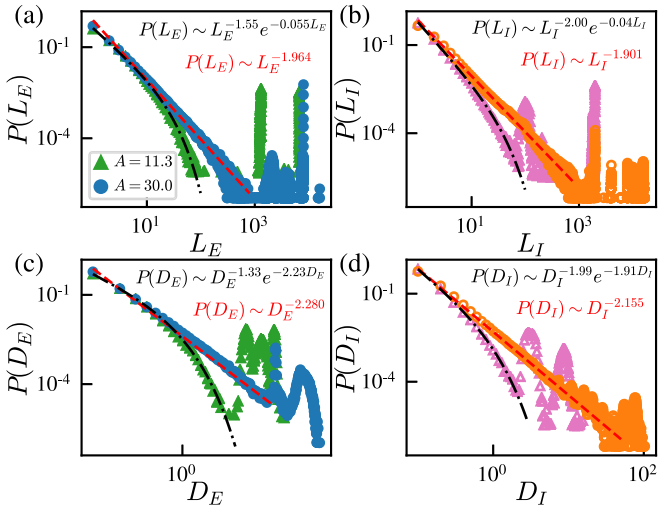

FIG. 4. Probability distributions of avalanche size $P(L_\alpha)$ and avalanche duration $P(D_\alpha)$ of excitatory and inhibitory neurons with $A = 11.3, 30.0$. Results are averaged over 100 independent realizations. The black dot-dashed lines: the fitting results by doing the least-squares fitting with the power-law forms with an exponential cutoff [Eqs. (15) and (16)]. The red dashed lines: the fitting results by doing the maximum likelihood estimator with the power-law forms [Eq. (17)]. The Kolmogorov-Smirnov distances are $\mathscr{D}_{L_E} = 0.015\,59$, $\mathscr{D}_{L_I} = 0.007\,40$, $\mathscr{D}_{D_E} = 0.008\,10$, and $\mathscr{D}_{D_I} = 0.003\,63$.

For $A_{c_2} < A \leqslant A_{c_3}$, the population activities show the firing patterns with multiple stripes [see Figs. 2(e5)–2(e7)]. The individual spikes are bursting with CV_α keeping a finite value larger than 1 [see Fig. 2(d)]. Since the continuous firing activities will result in the fast consumption of available neurotransmitters, the collective firing activity cannot emerge when the available neurotransmitters remain at extremely low levels as a result of the small recovery time. But the release fractions $u_i(t)$ of the available neurotransmitters remain high under intensive neuronal activities. The tradeoff between these processes results in the collective firing population activities with multiple stripes. Meanwhile, the synaptic inhibition can effectively reduce the phase difference between postsynaptic neurons by counteracting the synaptic excitation. Thus it is more likely to generate the strong bursty population activity after a brief accumulation of the available neurotransmitters [see Fig. 2(e7)]. We also find that the population activity in this bursty regime shows substantial trial-to-trial variability, and the periodic-like behavior can exist in short time series (see Figs. S7 and S8 in the Supplemental Material [45]). In this situation, the population activity is sensitivity to perturbations, similar to the previous findings from both experimental [2] and theoretical investigations [65]. A perturbation consisting of several extra spikes in the inactive period will lead to a phase advance of the collective firing activity of inhibitory neurons and a phase delay of excitatory ones. The aperiodic activity is more likely to emerge after

the cascading activities with large avalanche sizes, especially when the synaptic excitation from the pioneers is larger than a critical value [63]. Moreover, the avalanche size distributions $P(L_\alpha)$ and the avalanche duration distributions $P(D_\alpha)$ of the spike avalanches between the collective firing activities in this bursty regime (which are either entire or local periodic-like) display approximately the power-law forms

$$P(L_\alpha) \sim L_\alpha^{-\gamma_{L_\alpha}}, \quad P(D_\alpha) \sim D_\alpha^{-\gamma_{D_\alpha}}, \tag{17}$$

as shown in Fig. 4, where the exponents $\gamma_{L_\alpha}, \gamma_{D_\alpha}$ are estimated by doing the maximum likelihood estimator [66,67]. The Kolmogorov-Smirnov distances $\mathscr{D}_{L_\alpha}$ and $\mathscr{D}_{D_\alpha}$ between the data and the fit are small enough to ensure the reliability of the fitting. The exponents vary slightly with A because of the different synchronization degrees of the population activities, but they do not depend on the network size (see Fig. S6 and Table SII in the Supplemental Material [45]).

C. Pure spike-to-spike synchronization

When the synaptic efficacy A increases further and passes through A_{c_3}, the population activity experiences a tremendous change [see Fig. 2(a)]. The average firing rates r_α grow linearly with A, and the synchronization indexes S_α always remain at low levels in the interval $A_{c_3} < A \leqslant A_{c_4}^\alpha$ ($\alpha = E, I$), which indicates that the membrane potentials of neurons are usually in either a weakly synchronous or an asynchronous state. However, the Kuramoto parameter K_α of excitatory neurons decreases from a moderate value to zero, while that of the inhibitory neurons keeps a finite value. Clearly, these population activities only have the collective firing characteristic of *pure spike-to-spike synchronization*. In these patterns, the neurons fire intensively, and there exist firing neurons all the time, which rules out the presence of inactive periods under the temporal resolution of the dynamics [see Figs. 2(e8) and 2(e9)]. The average membrane potential oscillates with small amplitude, and the membrane potentials over neurons have large fluctuations all the time, finally resulting in the small S_α.

Raster plots in Figs. 2(e8) and 2(e9) show that it is difficult to extract information from the term series of spikes visually, hence it is necessary to analyze the population activity on a microscopic level. Figures 5(a) and 5(b) depict the bifurcation diagram of the time interval τ_α between two continuous collective firing stripes of excitatory and inhibitory neurons as a function of the synaptic efficacy A. The population activity displays a backward period-doubling transition from synchronous chaos to the periodic-like phase with period 4, 2, 1, with the increase of A. There is a narrow range in the chaotic region in which the attracting orbit is periodic-like (with period 4; see Fig. S9 in the Supplemental Material [45]). We discuss them separately below.

Irregular synchronous chaotic population activity. The strange global attractors in Fig. 5(c1) correspond to the macroscopic population activities that have the characteristic of synchronous chaos [68]. Both excitatory and inhibitory neurons fire collectively with low and high frequencies alternately, and the time intervals between two continuous collective firing stripes vary irregularly [see Figs. 5(a) and 5(b)]. The ISIs of each neuron vary greatly and distribute in a broad

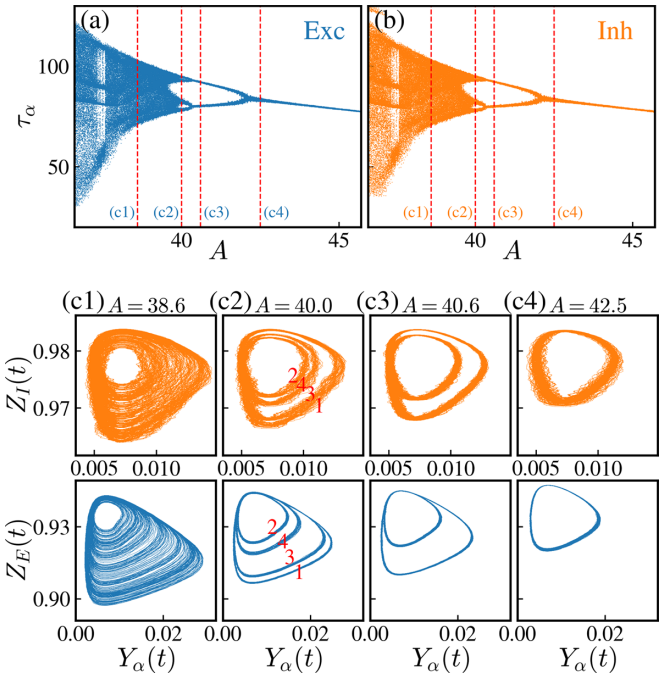

FIG. 5. (a), (b) Bifurcation diagram of the time interval τ_α between two continuous collective firing stripes of (a) excitatory and (b) inhibitory neurons as a function of the synaptic efficacy A. (c1)–(c4) Global attractors of excitatory (bottom) and inhibitory (top) neurons with $A =$ (c1) 38.6, (c2) 40.0, (c3) 40.6, and (c4) 42.5, corresponding to the red dashed lines in (a),(b). The red numbers in (c2) correspond to the collective firing activities marked by the same numbers in Fig. 6(b).

range without explicit characteristic ISIs [see Fig. 6(c)]. The firing patterns replotted by reordering the neurons according to their firing time in Fig. 6(a) show that the neurons fire gradually until all neurons have fired (because the synaptic currents of postsynaptic neurons are equal on average). Meanwhile, the firing orders of each neuron vary along the time with a small fluctuation among the neurons with relatively small differences of the firing times. The correlation between one ISI and the previous one of each neuron is small (see Fig. S10(a) in the Supplemental Material [45]).

Periodic-like population activities with period 4, 2, 1. For $A = 40.0$, the global attractors in Fig. 5(b) clarify the stable periodic-like population activities with period 4. After the most intensive collective firing of the excitatory and inhibitory neurons [as the highest maxima of the IPSRs $R_E(t)$ and $R_I(t)$ in Fig. 6(b)], synaptic excitation and inhibition from individual spikes of presynaptic neurons result in a large fluctuation of the membrane potentials. Then the neurons will fire in a cascading way until a collective firing activity occurs, and the second stripe is formed. Although the available neurotransmitters will fall to low levels after the bursty activities, the release fractions $u_i(t)$ of the available neurotransmitters give rise to high levels. The third collective firing occurs, and it is lower than the first one due to the consumption of available neurotransmitters, and higher than the second one due to the increase of the release fractions $u_i(t)$ and the decrease of the fluctuation of membrane potentials [see Fig. 6(b)]. Similarly, the fourth collective firing activity is higher than the

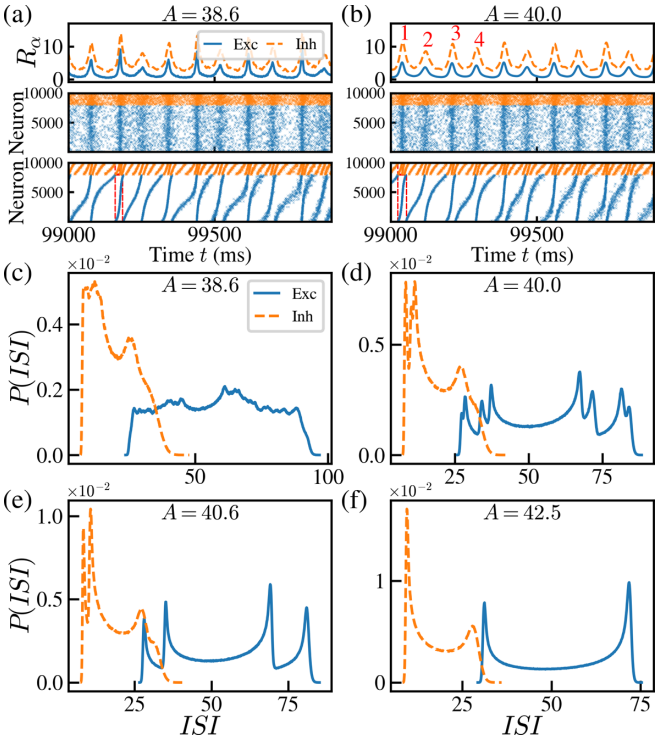

FIG. 6. (a), (b) Time series of the instantaneous population spike rate (IPSR) (top), raster plots (middle and bottom) for $A =$ (a) 38.6 and (b) 40.0. Neurons in the bottom ones are arranged vertically in order of firing time in the red rectangular areas. (c)–(f) Interspike-interval (ISI) distributions P(ISI) of excitatory and inhibitory neurons with $A =$ (c) 38.6, (d) 40.0, (e) 40.6, and (f) 42.5.

second one due to the accumulation of active neurotransmitters. These processes can be shown by the evolution of the closed orbits of average synaptic fields with different radius in Fig. 5(c2). With the increase of A, the third collective firing activity is enhanced until it reaches the same degree as the first one, finally leading to the periodic-like population activity with period two [see Fig. 5(c3)]. The switch process of the periodic-like behavior with period one from that with period two occurs with the similar pattern-formation dynamics [see Fig. 5(c4)].

Since the firing orders of each neuron vary along the time with a small fluctuation regardless of whether it is in the collective firing stripes or not (see Fig. 6(b)], the ISIs of the neurons in the firing patterns with period 4,2,1 are strongly correlated. Hence, the ISIs distribute in a broad range, and the ISI distributions display multimodal shapes, which is caused by the periodic-like population activity with characteristic ISIs of the neurons [see Figs. 6(b) and 6(d)–6(f)]. The existence of characteristic ISIs and the correlation between ISIs make sense to explain the closed curves of the ISI return map (see Figs. S10(b)– S10(d) in the Supplemental Material [45]).

D. Regular synchronous chaotic population activity

In the region $A^I_{c_4} < A \leqslant A^E_{c_4}$, the population activity of excitatory neurons shows pure spike-to-spike synchronization and periodic-like behavior with period 1, and the degree of synchronization decreases with the increase of A [see

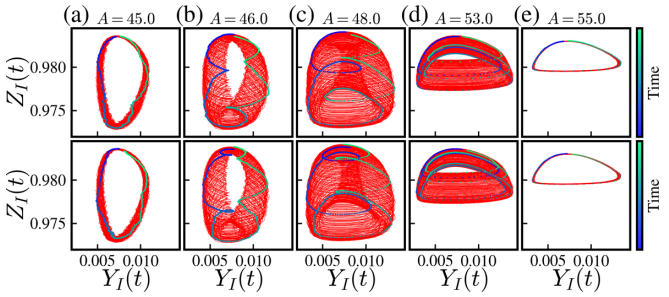

FIG. 7. Global attractors of inhibitory neurons with $A =$ (a) 45.0, (b) 46.0, (c) 48.0, (d) 53.0, and (e) 55.0. The red lines are the trajectories in the time window $85 < t \leqslant 90$ s. The color points are two consecutive evolutionary trajectories. Color encodes the time according to the color bar.

Figs. 2(b) and 2(c)]. However, the inhibitory neurons fire in a very complicated way. The fluctuations of global attractors of inhibitory neurons increase with A, and the trajectories are nonoverlapping but with certain regularity. The population activity evolves alternately with two different modes, as shown in Fig. 7. The difference between these two modes is the different number of collective firing activities whose average synaptic field $Y_I(t)$ decreases to the minimum (the left boundary of the global attractor). This interesting phenomenon implies the presence of the regular synchronous chaotic population activity. With the increase of A, the maxima of $Y_I(t)$ converge to the same value gradually, which indicates that the synchronization of collective firing stripes has the same intensity, but those of $Z_I(t)$ are different due to the slower recovery of available neurotransmitters [see Fig. 7(d)]. Furthermore, the difference between two such different modes decreases until reaching the periodic-like phase with regular spikes [see Fig. 7(e)].

E. Regular and asynchronous individual spikes

In the region $A > A^E_{c_4}$, both excitatory and inhibitory neurons fire with large firing rates as a result of the large synaptic efficacy (when excitation dominates inhibition with a small g). The ISIs of each neuron are so short that the available neurotransmitters $x_i(t)$ cannot recover from the inactive neurotransmitters $z_i(t)$ to large levels, and the active neurotransmitters $y_i(t)$ remain at low levels all the time. The presynaptic currents act as constant input with the large synaptic efficacy and have the same impact on the firings of excitatory neurons, which finally causes the asynchronous and regular firing activities of the excitatory neurons [see Fig. 2(e10)]. Meanwhile, since the inhibitory neurons are sensitive to synaptic excitation, the individual spikes of the excitatory neurons in an extremely brief period can lead to collective firing activities of inhibitory neurons, finally resulting in the synchronous and regular firing activities. In such a situation, the ISIs of both excitatory and inhibitory neurons are distributed according to Gaussian distributions with small variances [see Figs. 8(a) and 8(b)].

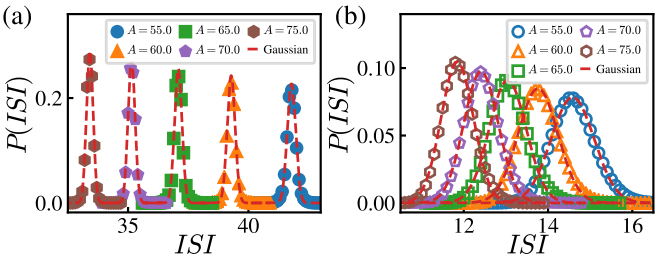

FIG. 8. Interspike-interval (ISI) distributions P(ISI) of (a) excitatory and (b) inhibitory neurons with $A = 55.0$, 60.0, 65.0, 70.0, and 75.0. The red dashed lines are Gaussian fits.

IV. SUMMARY AND DISCUSSION

In this paper, we have systematically investigated the population activity in the neuronal network composed of both excitatory and inhibitory neurons, which are equipped with short-term synaptic plasticity. Various collective firing patterns with different macroscopic properties emerge by varying the synaptic efficacy. The pattern-formation dynamics of these population activities are comprehensively discussed on a microscopic level.

The emergence of a mixed oscillatory pattern in the population activity displaying multiple stripes implies that both low and high oscillation frequencies are presented [58]. The low firing frequency of the whole mixed oscillatory pattern is caused by the large timescale of external drive and the short-term depression of synaptic plasticity after neuronal firing activities, while the high firing frequency of the fast oscillations in the firing patterns is due to the small timescale of synaptic interactions between neurons and the short-term facilitation of the synaptic plasticity.

Since the synaptic excitation is sufficient to induce the collective firing activities, we found that the inhibitory neurons can promote the generation of cluster firing behavior and strong bursty collective firing activity by depressing the activities of postsynaptic neurons partially or wholly, which increases the diversity of the population activity. The role of the inhibitory neurons in information processing is varied and complex and is actively being researched.

The bursty population activity features characteristic power-law distributed neuronal avalanches, and the neurons can fire collectively in either entire or local periodic-like ways. It is similar to the chaotic and bursty population activity with power-law scaling of activity events observed in the neuronal network of purely excitatory neurons [41]. We also found the neuronal avalanches in the power-law form with exponential cutoff in the irregular (excitatory neurons) and bursty (inhibitory neurons) regimes. The distributions get close to the power-law forms gradually with the increase of the synaptic efficacy. However, the exponents are variable in different situations, and there are still many puzzles waiting for further investigations [69]. The power-law avalanches provide deep insight to the studies of criticality, where the power law is a necessary but not sufficient condition of critical behavior.

In addition, the pure spike-to-spike synchronous population activities are found in a specific range, where the neurons fire with large firing rates, and there are firing neurons all the time, which rules out the presence of inactive periods. The collective firing activity cannot emerge when the available neurotransmitters stay at extremely low levels under intensive neuronal activities, where the system will transition from the bursty regime to the asynchronous regime. However, the bifurcation diagram of the time interval τ_α between two continuous collective firing stripes shows that the periodic-like phase emerges from the synchronous chaos after the backward period-doubling transition. The stable periodic-like phases of the population activities, both weakly and intensively, are robust to the perturbations consisting of several extra spikes at any time and any individual, which are helpful for neural code. However, the local periodic-like and (regular or irregular) synchronous chaotic phases display substantial trial-to-trial variability, which will have the opposite effect.

We have also investigated the case of strong external drives in the Supplemental Material (Sec. SIII) [45]. Since the activities of excitatory neurons are enhanced with strong external drive, synaptic excitation increases and promotes the population activities by canceling out the synaptic inhibition, and the regions where inhibition dominates excitation reduce or disappear. For strong enough external drive, the available neurotransmitters are so low under intensive neuronal activities that the firing patterns (displaying pure spike-to-spike synchronization) are impossible to generate. Moreover, the parametric regions with similar pattern-formation dynamics separate obviously when we increase the spontaneous activities of excitatory neurons. The asynchronous population activities emerge and the synchronous population activities can only be found within some limited parameter ranges.

The synchronous oscillations have been heavily studied by a lot of different models to explore the pattern formation from experimental studies [39], the brain ability to perform cognitive functions [65], the pathological mechanism and effective treatment of brain diseases [63], etc. In the field of neuroscience, the recent advent of measuring techniques such as electroencephalogram, electrocorticogram, magnetoencephalography, high-density multielectrode recording, and

TABLE I. Parameters for neuronal membrane dynamics of adaptive exponential integrate-and-fire excitatory neurons and standard leaky integrate-and-fire inhibitory neurons [50].

Symbol	Description	Value
τ_m	Membrane time constant	20 ms
V^E_{rest}	Excitatory neuron resting potential	−70 mV
V^I_{rest}	Inhibitory neuron resting potential	−62 mV
Δ_T	Spike slope factor	2 mV
C	Membrane capacitance	300 pF
τ_T	Adaptive threshold timescale	30 ms
V_{th}	Threshold potential	−52 mV
A_T	Post spike threshold potential increase	10 mV
τ_w	Spike-triggered adaptation timescale	150 ms
a_w	Level of subthreshold adaptation	4 nS
b_w	Spike-triggered adaptation	0.805 pA
θ^E	Excitatory neuron firing threshold	20 mV
θ^I	Inhibitory neuron firing threshold	−52 mV
V_{r}	Reset potential	−60 mV
τ_{ref}	Refractory period	2 ms

TABLE II. Parameters for the short-term synaptic plasticity governed by the Tsodyks-Uziel-Markram model [39,53].

Symbol	Description	Value
τ_{in}	Characteristic decay time of active neurotransmitter	6 ms
τ_r	Recovery time of available neurotransmitter from inactive neurotransmitter	798 ms
τ_{fac}	Characteristic time for the calcium channel gates to transit from the open state to the closed state	1000 ms
U	Release fraction at rest	0.1

two-photon imaging has made it easier to measure neuronal activity, promoting the development of neuroscience [70,71]. If any similar firing patterns are found experimentally, we may be able to explore the intrinsic mechanism by adjusting parameters in our neuronal network. The undiscovered phenomena that have not been studied completely can also be predicted. We hope that our presented results can improve the understanding of the diverse features and the neuronal mechanisms of the various collective firing population activities and eventually open up a promising avenue for therapeutics of brain diseases.

ACKNOWLEDGMENTS

We would like to thank Xu-Sheng Liu for fruitful discussions. This work was supported by the National Natural Science Foundation of China (Grants No. 11975111 and No. 12047501).

APPENDIX A: PARAMETERS

Parameter values for the neuronal membrane dynamics and the synaptic current used in our simulations are listed in Tables I and II, respectively.

APPENDIX B: MACROSCOPIC POPULATION ACTIVITY IN THE PARAMETER SPACE OF A AND g

Figure 9 shows the average firing rates r_α, the synchronization indexes S_α, and the Kuramoto parameters K_α of both excitatory ($\alpha = E$) and inhibitory ($\alpha = I$) neurons in a neuronal network with $I^{E,\text{ext}} = 314$ pA and $I^{I,\text{ext}} = 150$ pA. The neurons fire more intensively in the region with small g or small A (which is exhibited by relatively large r_α), and they are suppressed in the region with large g and large A. The statistical indicators oscillate with the change of the parameters. The average firing rate of inhibitory neurons is higher than that of excitatory neurons in most of the parameter

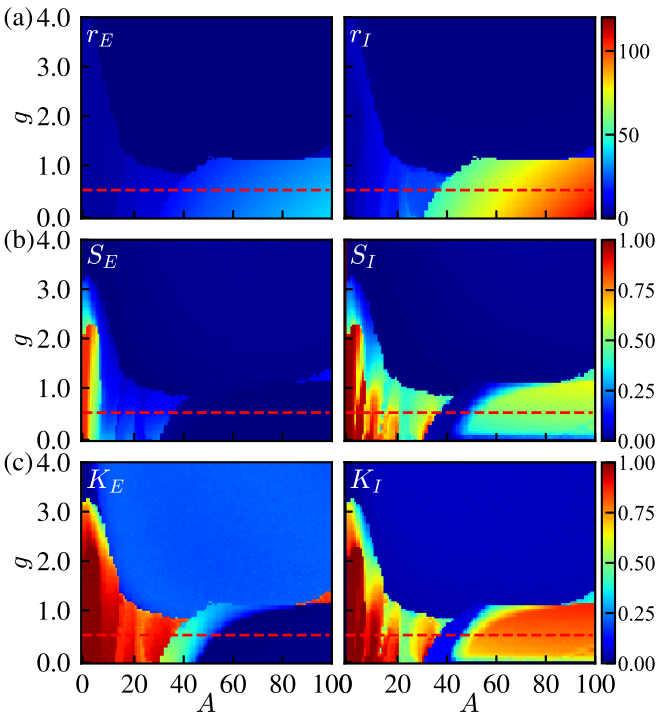

FIG. 9. (a) Average firing rates r_α, (b) synchronization indexes S_α, and (c) Kuramoto parameter K_α of excitatory ($\alpha = E$) and inhibitory ($\alpha = I$) neurons in the parameter space of synaptic efficacy A and relative inhibitory efficacy g. The constant external input currents of excitatory and inhibitory neurons are $I^{E,\text{ext}} = 314$ pA and $I^{I,\text{ext}} = 150$ pA, respectively. The red dashed lines correspond to $g = 0.5$.

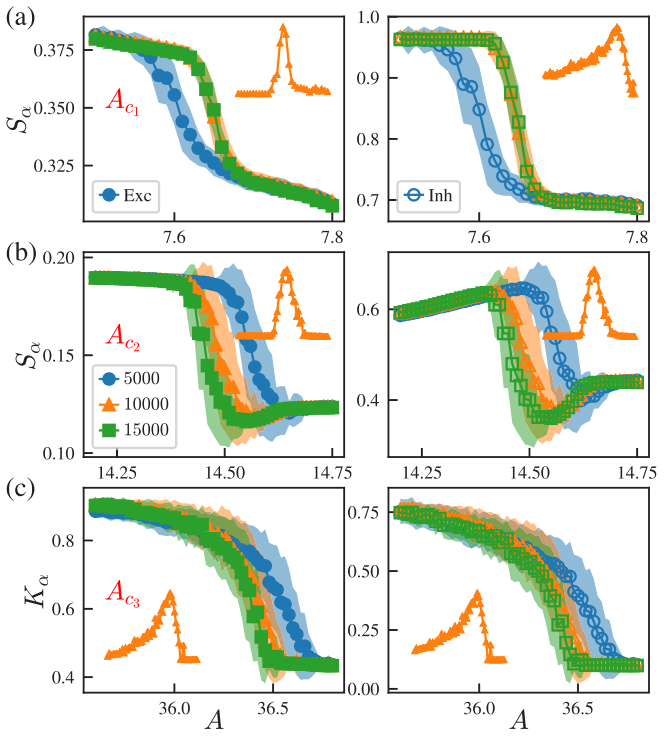

FIG. 10. (a), (b) Synchronization indexes S_α, and (c) Kuramoto parameter K_α of excitatory (left) and inhibitory (right) neurons near the transition points A_{c_1}, A_{c_2}, and A_{c_3} with different network size N. Results for $N = 5000$ and 10 000 are averaged over 100 independent realizations; others are averaged over 50 independent realizations. The shaded regions are the standard deviations. The insets are the standard deviations for $N = 10\,000$.

space, which means that the population activity of inhibitory neurons is more intensive than excitatory neurons. Moreover, the average firing rate of inhibitory neurons is always positive proportional to that of the excitatory neurons, which implies that the activities of the inhibitory neurons and the excitatory neurons are correlated.

Since the synaptic inhibition from inhibitory neurons grows with the increase of g, the generation of other stripes following the front one becomes more difficult, finally resulting in the gradual disappearance of some stripes. In this case, the average firing rates decrease with the increase of g. The total presynaptic current even becomes negative with large g (when inhibition dominates excitation), and depresses the population activity into a weak one [see Fig. 9(a)]. It is strange and counterintuitive to observe that the firing rate and synchronous behavior for large g weakens as A increases. The inhibitory neurons are more sensitive than excitatory neurons to the synaptic excitation, which is confirmed by the response to the input currents with the small intensity (data not shown). The effect of synaptic inhibition grows with the increase of A due to the larger firing rates of inhibitory neurons. Then, such a negative effect from inhibitory neurons counteracts the external drive and the synaptic excitation, and then depresses the whole system remarkably.

APPENDIX C: THE TRANSITION POINTS

The curves of statistical indicators (r_α, S_α, and K_α) in Fig. 2 show that there are lots of transition points for excitatory and inhibitory neurons, either separately or jointly, and they separate the regions with similar pattern-formation dynamics. We only list some of the transition points that are convenient for analyzing and discussing the pattern-formation dynamics. Results show that r_α, S_α, and K_α near the transition points $A_{c_1}, A_{c_2}, A_{c_3}$ are dependent on the network size N (with the finite-size effects), and they will converge to the stationary one in the limit $N \to \infty$. Meanwhile, the fluctuations at transition points are maximum. We only display some results in Fig. 10 as a demonstration; all other results can be found in Fig. S1 in the Supplemental Material [45].

[1] D. J. Amit and N. Brunel, Model of global spontaneous activity and local structured activity during delay periods in the cerebral cortex, Cereb. Cortex **7**, 237 (1997).

[2] M. London, A. Roth, L. Beeren, M. Häusser, and P. E. Latham, Sensitivity to perturbations in vivo implies high noise and suggests rate coding in cortex, Nature (London) **466**, 123 (2010).

[3] J. M. Beggs and D. Plenz, Neuronal avalanches in neocortical circuits, J. Neurosci. **23**, 11167 (2003).

[4] T. Bellay, A. Klaus, S. Seshadri, and D. Plenz, Irregular spiking of pyramidal neurons organizes as scale-invariant neuronal avalanches in the awake state, eLife **4**, e07224 (2015).

[5] T. Petermann, T. C. Thiagarajan, M. A. Lebedev, M. A. L. Nicolelis, D. R. Chialvo, and D. Plenz, Spontaneous cortical activity in awake monkeys composed of neuronal avalanches, Proc. Natl. Acad. Sci. USA **106**, 15921 (2009).

[6] G. Buzsáki and A. Draguhn, Neuronal oscillations in cortical networks, Science **304**, 1926 (2004).

[7] G. Buzsáki, *Rhythms of the Brain* (Oxford University Press, New York, 2006).

[8] D.-P. Yang, H.-J. Zhou, and C. Zhou, Co-emergence of multi-scale cortical activities of irregular firing, oscillations and avalanches achieves cost-efficient information capacity, PLoS Comput. Biol. **13**, e1005384 (2017).

[9] C. van Vreeswijk and H. Sompolinsky, Chaos in neuronal networks with balanced excitatory and inhibitory activity, Science **274**, 1724 (1996).

[10] A. Renart, J. de la Rocha, P. Bartho, L. Hollender, N. Parga, A. Reyes, and K. D. Harris, The asynchronous state in cortical circuits, Science **327**, 587 (2010).

[11] J. M. Beggs and D. Plenz, Neuronal avalanches are diverse and precise activity patterns that are stable for many hours in cortical slice cultures, J. Neurosci. **24**, 5216 (2004).

[12] C. W. Eurich, J. M. Herrmann, and U. A. Ernst, Finite-size effects of avalanche dynamics, Phys. Rev. E **66**, 066137 (2002).

[13] J.-n. Teramae and T. Fukai, Local cortical circuit model inferred from power-law distributed neuronal avalanches, J. Comput. Neurosci. **22**, 301 (2007).

[14] A. Levina, J. M. Herrmann, and T. Geisel, Dynamical synapses causing self-organized criticality in neural networks, Nat. Phys. **3**, 857 (2007).

[15] P. Moretti and M. A. Muñoz, Griffiths phases and the stretching of criticality in brain networks, Nat. Commun. **4**, 2521 (2013).

[16] R. Legenstein and W. Maass, Edge of chaos and prediction of computational performance for neural circuit models, Neural Netw. **20**, 323 (2007).

[17] C. Haldeman and J. M. Beggs, Critical Branching Captures Activity in Living Neural Networks and Maximizes the Number of Metastable States, Phys. Rev. Lett. **94**, 058101 (2005).

[18] W. L. Shew, H. Yang, S. Yu, R. Roy, and D. Plenz, Information capacity and transmission are maximized in balanced cortical networks with neuronal avalanches, J. Neurosci. **31**, 55 (2011).

[19] O. Kinouchi and M. Copelli, Optimal dynamical range of excitable networks at criticality, Nat. Phys. **2**, 348 (2006).

[20] W. L. Shew, H. Yang, T. Petermann, R. Roy, and D. Plenz, Neuronal avalanches imply maximum dynamic range in cortical networks at criticality, J. Neurosci. **29**, 15595 (2009).

[21] C.-Y. Wang, Z.-X. Wu, and M. Z. Q. Chen, Approximate-master-equation approach for the Kinouchi-Copelli neural model on networks, Phys. Rev. E **95**, 012310 (2017).

[22] D. R. Chialvo, Emergent complex neural dynamics, Nat. Phys. **6**, 744 (2010).

[23] T. Mora and W. Bialek, Are biological systems poised at criticality?, J. Stat. Phys. **144**, 268 (2011).

[24] D. Plenz and E. Niebur, *Criticality in Neural Systems* (Wiley-VCH Verlag, Weinheim, Germany, 2014).

[25] A. Pikovsky, M. Rosenblum, and K. Jürgen, *Synchronization: A Universal Concept in Nonlinear Sciences* (Cambridge University Press, Cambridge, UK, 2001).

[26] G. V. Osipov, J. Kurths, and C. Zhou, *Synchronization in Oscillatory Networks*, Springer Series in Synergetics (Springer, Berlin, 2007).

[27] X.-J. Wang, Neurophysiological and computational principles of cortical rhythms in cognition, Physiol. Rev. **90**, 1195 (2010).

[28] M. E. Hasselmo, What is the function of hippocampal theta rhythm?-linking behavioral data to phasic properties of field potential and unit recording data, Hippocampus **15**, 936 (2005).
[29] N. Swann, N. Tandon, R. Canolty, T. M. Ellmore, L. K. McEvoy, S. Dreyer, M. DiSano, and A. R. Aron, Intracranial EEG reveals a time- and frequency-specific role for the right inferior frontal gyrus and primary motor cortex in stopping initiated responses, J. Neurosci. **29**, 12675 (2009).
[30] P. Fries, Neuronal gamma-band synchronization as a fundamental process in cortical computation, Annu. Rev. Neurosci. **32**, 209 (2009).
[31] M. Steriade, *Neuronal Substrates of Sleep and Epilepsy* (Cambridge University Press, Cambridge, UK, 2003).
[32] P. J. Uhlhaas and W. Singer, Abnormal neural oscillations and synchrony in schizophrenia, Nat. Rev. Neurosci. **11**, 100 (2010).
[33] P. J. Uhlhaas and W. Singer, Neural synchrony in brain disorders: Relevance for cognitive dysfunctions and pathophysiology, Neuron **52**, 155 (2006).
[34] D. Purves, G. J. Augustine, D. Fitzpatrick, W. C. Hall, A.-S. LaMantia, J. O. McNamara, and L. E. White, *Neuroscience*, 4th ed. (Sinauer Associates, Sunderland, MA, 2008).
[35] E. R. Kandel, J. H. Schwartz, T. M. Jessell, S. A. Siegelbaum, and A. J. Hudspeth, *Principles of Neural Science*, 5th ed. (McGraw-Hill Medical, New York, 2013).
[36] M. Tsodyks, A. Uziel, and H. Markram, Synchrony generation in recurrent networks with frequency-dependent synapses, J. Neurosci. **20**, RC50 (2000).
[37] H. Markram and M. Tsodyks, Redistribution of synaptic efficacy between neocortical pyramidal neurons, Nature (London) **382**, 807 (1996).
[38] M. V. Tsodyks and H. Markram, The neural code between neocortical pyramidal neurons depends on neurotransmitter release probability, Proc. Natl. Acad. Sci. USA **94**, 719 (1997).
[39] M. di Volo, R. Livi, S. Luccioli, A. Politi, and A. Torcini, Synchronous dynamics in the presence of short-term plasticity, Phys. Rev. E **87**, 032801 (2013).
[40] E. Bertolotti, R. Burioni, M. di Volo, and A. Vezzani, Synchronization and long-time memory in neural networks with inhibitory hubs and synaptic plasticity, Phys. Rev. E **95**, 012308 (2017).
[41] F. Pittorino, M. Ibáñez-Berganza, M. di Volo, A. Vezzani, and R. Burioni, Chaos and Correlated Avalanches in Excitatory Neural Networks with Synaptic Plasticity, Phys. Rev. Lett. **118**, 098102 (2017).
[42] S. Luccioli, D. Angulo-Garcia, R. Cossart, A. Malvache, L. Módol, V. H. Sousa, P. Bonifazi, and A. Torcini, Modeling driver cells in developing neuronal networks, PLoS Comput. Biol. **14**, 1 (2018).
[43] P.-X. Lin, C.-Y. Wang, and Z.-X. Wu, Two-fold effects of inhibitory neurons on the onset of synchronization in izhikevich neuronal networks, Eur. Phys. J. B **92**, 113 (2019).
[44] V. Volman, I. Baruchi, E. Persi, and E. Ben-Jacob, Generative modeling of regulated dynamical behavior in cultured neuronal networks, Physica A **335**, 249 (2004).
[45] See Supplemental Material at http://link.aps.org/supplemental/10.1103/PhysRevE.103.022312 for more details of calculations, analysis and simulational results.
[46] D. L. Meinecke and A. Peters, GABA immunoreactive neurons in rat visual cortex, J. Comp. Neurol. **261**, 388 (1987).
[47] N. Brunel, Dynamics of sparsely connected networks of excitatory and inhibitory spiking neurons, J. Comp. Neurosci. **8**, 183 (2000).
[48] R. Brette and W. Gerstner, Adaptive exponential integrate-and-fire model as an effective description of neuronal activity, J. Neurophysiol. **94**, 3637 (2005).
[49] L. Badel, S. Lefort, R. Brette, C. C. H. Petersen, W. Gerstner, and M. J. E. Richardson, Dynamic I-V curves are reliable predictors of naturalistic pyramidal-neuron voltage traces, J. Neurophys. **99**, 656 (2008).
[50] A. Litwin-Kumar and B. Doiron, Formation and maintenance of neuronal assemblies through synaptic plasticity, Nat. Commun. **5**, 5319 (2014).
[51] W. Gerstner, W. M. Kistler, R. Naud, and L. Paninski, *Neuronal Dynamics: From Single Neurons to Networks and Models of Cognition* (Cambridge University Press, Cambridge, UK, 2014).
[52] C.-C. Chen and D. Jasnow, Event-driven simulations of a plastic, spiking neural network, Phys. Rev. E **84**, 031908 (2011).
[53] A. Levina, J. M. Herrmann, and T. Geisel, Phase Transitions Towards Criticality in a Neural System with Adaptive Interactions, Phys. Rev. Lett. **102**, 118110 (2009).
[54] M. Uzuntarla, J. J. Torres, P. So, M. Ozer, and E. Barreto, Double inverse stochastic resonance with dynamic synapses, Phys. Rev. E **95**, 012404 (2017).
[55] M. Nawrot, A. Aertsen, and S. Rotter, Single-trial estimation of neuronal firing rates: From single-neuron spike trains to population activity, J. Neurosci. Meth. **94**, 81 (1999).
[56] H. Shimazaki and S. Shinomoto, Kernel bandwidth optimization in spike rate estimation, J. Comput. Neurosci. **29**, 171 (2010).
[57] S.-Y. Kim and W. Lim, Fast sparsely synchronized brain rhythms in a scale-free neural network, Phys. Rev. E **92**, 022717 (2015).
[58] D. Guo, Q. Wang, and M. Perc, Complex synchronous behavior in interneuronal networks with delayed inhibitory and fast electrical synapses, Phys. Rev. E **85**, 061905 (2012).
[59] F. A. Rodrigues, T. K. D. Peron, P. Ji, and J. Kurths, The Kuramoto model in complex networks, Phys. Rep. **610**, 1 (2016).
[60] The *firing pattern* denoted in our paper is the population activity in a relatively small time window, which characterizes the temporal response of the whole system and will repeat in long time series of the spikes, such as the population activity of the periodic-like behavior in one period.
[61] B. J. Richmond, L. M. Optican, M. Podell, and H. Spitzer, Temporal encoding of two-dimensional patterns by single units in primate inferior temporal cortex. i. response characteristics, J. Neurophys. **57**, 132 (1987).
[62] R. Zillmer, N. Brunel, and D. Hansel, Very long transients, irregular firing, and chaotic dynamics in networks of randomly connected inhibitory integrate-and-fire neurons, Phys. Rev. E **79**, 031909 (2009).
[63] J. D. Touboul, C. Piette, L. Venance, and G. B. Ermentrout, Noise-Induced Synchronization and Antiresonance in Interacting Excitable Systems: Applications to Deep Brain Stimulation in Parkinson's Disease, Phys. Rev. X **10**, 011073 (2020).
[64] In this situation, the pioneers will fire again with relatively short ISIs with the large synaptic currents after the collective firing

activity of the excitatory neurons. And they will fire first in the next inactive period because they integrate relatively less inhibitory currents when they go through the absolute refractory periods. Thus the pioneers that drive the neuronal cascades are fixed (see Fig. S4 in the Supplemental Material [45]).

[65] M. Monteforte and F. Wolf, Dynamic Flux Tubes Form Reservoirs of Stability in Neuronal Circuits, Phys. Rev. X **2**, 041007 (2012).

[66] A. Clauset, C. Shalizi, and M. Newman, Power-law distributions in empirical data, SIAM Rev. **51**, 661 (2009).

[67] J. Alstott, E. Bullmore, and D. Plenz, Powerlaw: A python package for analysis of heavy-tailed distributions, PLoS ONE **9**, e85777 (2014).

[68] D. Battaglia and D. Hansel, Synchronous chaos and broad band gamma rhythm in a minimal multi-layer model of primary visual cortex, PLoS Comput. Biol. **7**, e1002176 (2011).

[69] A. J. Fontenele, N. A. P. de Vasconcelos, T. Feliciano, L. A. A. Aguiar, C. Soares-Cunha, B. Coimbra, L. Dalla Porta, S. Ribeiro, A. J. A. Rodrigues, N. Sousa, P. V. Carelli, and M. Copelli, Criticality between Cortical States, Phys. Rev. Lett. **122**, 208101 (2019).

[70] I. H. Stevenson and K. P. Kording, How advances in neural recording affect data analysis, Nat. Neurosci. **14**, 139 (2011).

[71] G. Hong and C. M. Lieber, Novel electrode technologies for neural recordings, Nat. Rev. Neurosci. **20**, 330 (2019).